

OROGRAPHIC PRECIPITATION MECHANISMS: NEW DATA FROM THE MESOSCALE ALPINE PROGRAMME

Robert A. Houze, Jr.,* Socorro Medina, and Sandra E. Yuter
Department of Atmospheric Sciences, University of Washington, USA

1. INTRODUCTION

Smith (1979) reviewed the basic ways in which upslope flow can affect precipitation formation and fall-out. He suggested that to a first approximation, orographic precipitation is equal to the moisture condensed as a layer of air ascends over the windward side of the terrain. This simple view assumes that as soon as moisture condenses in the upslope flow, it immediately falls to the ground as precipitation. Such a process would be 100 percent efficient. One way to evaluate orographic precipitation is by how closely it achieves Smith's simplified model.

One of the factors identified by Smith (1979) is the stability of the flow impinging on a mountain barrier. The Mesoscale Alpine Programme (MAP) in the European Alps in autumn 1999 (Bougeault et al. 2000) documented heavy orographic rain events in which the upstream flow stability ranged from absolutely stable to weakly potentially unstable. This paper reviews highlights of those cases and presents an emerging conceptual model of the orographic precipitation mechanisms under these conditions. We also point out the need to explore the precipitation mechanisms in orographic regimes characterized by stronger instability, as occurs over the mountains of Taiwan.

2. TWO OROGRAPHIC RAINSTORMS IN MAP: A STABLE CASE AND A WEAKLY UNSTABLE CASE

Major precipitation and flooding occur on the Mediterranean side of the Alps during autumn, when midlatitude baroclinic waves move across the region. A strong southeasterly flow of moist air at low levels on the eastern side of the approaching trough advects warm, moist air from the Mediterranean up and over the Alpine barrier. Figure 1 shows the topography of the Alps in relation to the Mediterranean Sea. The big M marks the Lago Maggiore region, where radar data were obtained. The location of Milano is shown, where soundings were taken upstream of the Alps.

Figure 2 shows the average Milano sounding for two major rain systems. The storm of 19-21 September 1999 (IOP2b) had precipitation amounts up to ~200-300 mm, while the storm of 20-21 October 1999 (IOP8) had accumulations up to ~70-80 mm in the Lago Maggiore re-

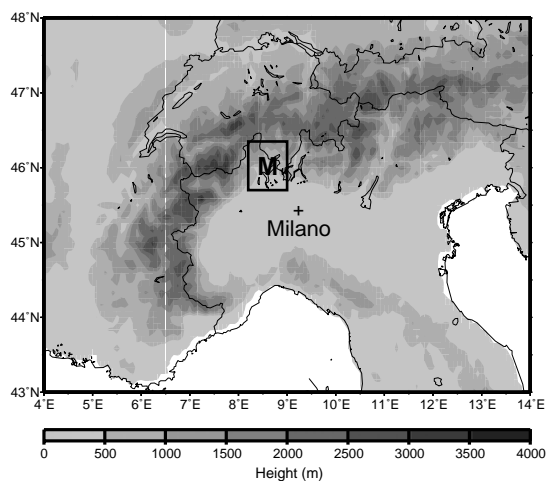


Figure 1. Topography over the Alps. See text for a description of symbols.

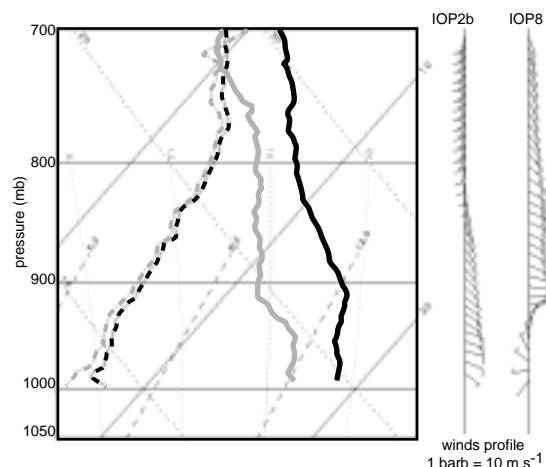


Figure 2. Storm mean sounding for MAP IOP2b and IOP8. Data taken at Milano-Linate Airport, Italy. Temperature (black) and dewpoint (gray) soundings for IOP2b (heavy solid) and IOP8 (heavy dashed) plotted on skew-T log p diagram. Solid sloping lines are temperature in °C. Sloping short dashed lines are dry adiabats labeled in °C. Long dashed lines are saturation mixing ratio in g kg^{-1} . Dotted lines are moist adiabats labeled in wet-bulb potential temperature in °C.

gion. IOP8 was a very stable case, relatively cool, with weak winds at low levels (surface to 900 mb). IOP2b was potentially unstable, warmer, and had strong winds at low levels. Both cases had strong southeasterly winds (toward the Alpine mountain barrier) above 900 mb. The

*Corresponding author address: Professor R. A. Houze, Jr., Atmospheric Sciences, Box 351640, University of Washington, Seattle, WA 98195-1640, USA. email: houze@atmos.washington.edu

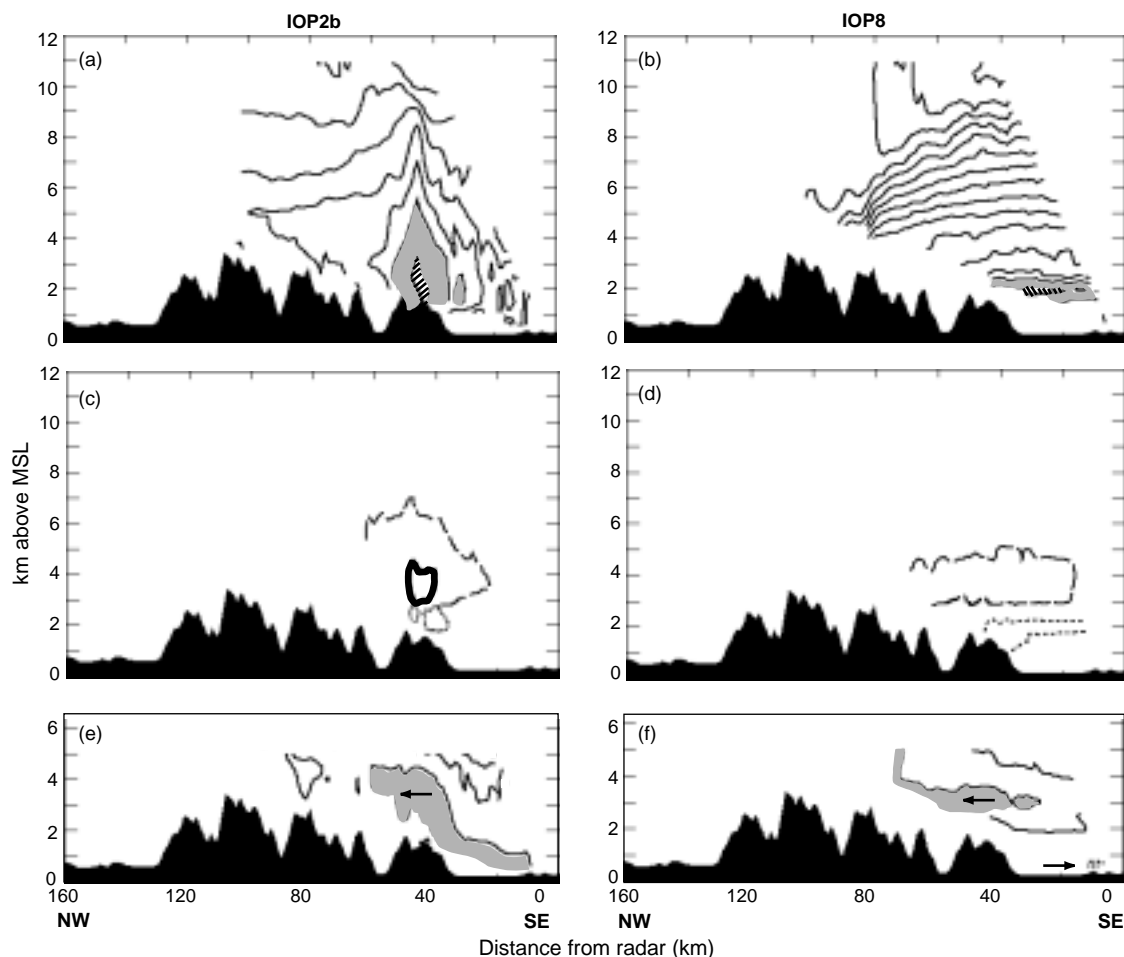


Figure 3. Southeast-northwest vertical cross section of S-Pol radar data. The section extends 160 km from the S-Pol radar, which was located at the southeast end of the cross section. The fields in the cross section panels have been either accumulated or averaged over 1500-1900 UTC 20 Sept 1999 for IOP2b and 0810-0850 UTC 21 Oct 1999 for IOP8. (a)-(b) Mean reflectivity. IOP2b: contours every 10 dBZ, dBZ = 32-42 shaded, dBZ > 42 hatched. IOP8: contours every 4 dBZ, dBZ = 30.5-34.5 shaded, dBZ > 34.5 hatched. (c)-(d) Particle types identified by polarimetric radar algorithms. Contours enclose regions of frequency of occurrence of dry snow (long dashed: IOP2b, 0.15; IOP8, 0.85) wet snow (short dashed: IOP2b, 0.08; IOP8, 0.40), and graupel (solid: IOP2b, 0.13). (e)-(f) Mean radial velocity. IOP2b: > 12 m s⁻¹ shaded; IOP8: > 19.5 12 m s⁻¹ shaded. Negative contour shown: -0.5, -3 m s⁻¹. Solid contours indicate flow towards the radar; dashed lines indicate flow away from it. Arrows indicate direction of horizontal component of radial velocity.

deeper layer of flow toward and over the terrain in IOP2b together with its warmth and greater instability all led to the heavier rain in that case. Houze et al. (2000) described the differences in wind, stability, and temperature in these two cases. Houze and Medina (2001) reported the microphysical differences between the two cases as indicated by the S-Pol polarimetric radar. Yuter and Houze (2001) examined vertically pointing radar data and carried out simple model calculations that help understand the microphysical differences. In this paper we summarize these previously reported results and present a conceptual model that accounts for the different mechanisms of precipitation growth in the stable (IOP8) case and the weakly unstable case (IOP2b).

3. POLARIMETRIC RADAR OBSERVATIONS IN THE STABLE AND UNSTABLE CASES

Figure 3 shows the airflow, precipitation, and microphysics in a vertical cross section extending southeast to northwest from the S-Pol radar northwestward up to the summit of the Alps. This section lies roughly parallel to the flow at the 2-km level. All the figures are mean or composite patterns. Figures 3a, c, and e contain data from the S-Pol radar for IOP2b (1500-1900 UTC 20 September). Figures 3b, d, and f contain data from the S-Pol radar for IOP8 (0810-0850 UTC 21 October 1999). Cross sections averaged over the whole storm are qualitatively similar but less amplified.

The mean reflectivity field (Fig. 3a) shows a well-defined convective echo structure (maximum echo > 40 dBZ) over the first peak of the mountain range, where the horizontal gradient of elevation first becomes very large. Smaller and weaker convective echo maxima appear just upwind of the major cell over the terrain. The major maximum over the first peak of the range is the cumulative effect of cells preferentially forming over the peak of the terrain. Time-lapse sequences of the low-level constant-altitude echo patterns at 5-min intervals suggest that the small, weaker, average cellular structures just upwind were produced by transient northward-propagating cells, which were not tied closely to the terrain.

Particle-identification algorithms (Vivekanandan et al. 1999) were applied to S-Pol dual-polarization radar data. The outputs of the algorithm were accumulated over the 4-h time period of the cross sections in Fig. 3c. The contours surround the regions of frequency of occurrence of three types of ice particles: graupel, wet snow, and dry snow. The solid contours indicate that graupel occurred preferentially above the first major mountain peak, directly above the reflectivity maximum seen in Fig. 3a. Dry snow (long-dashed contours) surrounded the graupel. The dry snow is just one category of dry ice particles identified by the polarimetric algorithm; the remainder of the echo volume seen in Fig. 3a above the 0°C level consists of ice particles associated with lower reflectivities. The small region of wet snow identified by the polarimetric data (dotted contours) was evidently produced by the melting of the graupel—the maximum of graupel occurrence was above the melting level, while the reflectivity (heaviest rain) maximum lay just below. The maximum of graupel occurrence directly over the precipitation maximum seen in the reflectivity suggests that riming of ice particles just above the 0°C level and their subsequent fallout and melting may have been a major factor contributing to the reflectivity maximum at lower levels. The data in Figs. 3a and c thus suggest that both riming and coalescence played an important role in producing high precipitation accumulations over the lower windward portion of the Alps during IOP2b. The graupel evidently occurred as a result of the recurrent convective updrafts producing supercooled water over the mountain peak. The ice particles growing in the convective cells over the mountain peak probably grew quickly into graupel particles by collecting the supercooled water and quickly fell into the warmer layer below, where they melted and became part of the heavy rain producing the peak echo in Fig. 3a.

The radial velocity pattern in IOP2b (Fig. 3e) shows that the most frequent occurrence of graupel was over the first major peak in the topography at the downwind end of a radial velocity jet directed toward, up, and over the terrain. A low-level jet flowed to the mountains from the Po Valley and rose over the terrain when the airflow encountered the first major peak. This persistent jet of Mediterranean air transported moisture above the 0°C level and released potential instability preferentially in

its rise up to the first major peak in the terrain. This mechanism would have saturated and condensed cloud liquid water, which was collected by raindrops below the 0°C level and accreted by ice particles above the freezing level. The accretion by ice particles of supercooled cloud liquid water condensed and transported by the jet up the terrain then led to the maximum of graupel occurrence seen in Fig. 3c.

In contrast to IOP2b, the precipitation in IOP8 (Fig. 3b) had a stratiform structure. The echo was weaker (maximum ~34 dBZ), and a distinct bright band at the 2-km level extended upstream of the Alpine range. The particle identification during IOP8 (Fig. 3d) also exhibited a horizontally layered structure, characterized by wet snow in the melting layer with dry snow above. The S-Pol radar detected no evidence of graupel whatsoever in this case. The radial velocity structure in IOP8 (Fig. 3f) contained an elevated jet around 3 km but it did not slope upward, and thus did not indicate any vertical motion at low levels, as was the case in IOP2b (cf. Fig. 3e). At low levels the radial component of the flow was toward the radar, indicating a return or blocked flow over the Po Valley. This blocked flow was evident in the soundings (weak wind at low levels in IOP8 in Fig. 2). It was also seen in data from the Doppler on Wheels (DOW), a mobile ground-based Doppler radar located in valleys (Houze et al. 2000), and in airborne dual-Doppler radar data (Bousquet and Smull 2001; Smull et al. 2001).

4. MODELING RESULTS

Yuter and Houze (2001) analyzed vertically pointing Doppler-radar observations obtained in IOP2b to obtain typical vertical velocities in the convective cells observed over the windward peaks of the Alps in that case. The peak vertical velocities ranged from 2–5 m s⁻¹. Using a simple ice-phase microphysical parameterization, they calculated the mixing ratios of hydrometeor species in parcels rising through these altitudes at the observed vertical velocities. They calculated mixing ratios of water vapor (q_v), cloud water (q_c), rain (q_r), and ice (q_i). The microphysical processes included in the calculations were: condensation of cloud water C_c , autoconversion A_c (the rate at which cloud water content decreases as a result of growth of precipitation by coalescence of cloud drops), collection of cloud water by raindrops K_c , collection of cloud water by graupel above the 0°C level K_{ci} , the glaciation of rain into ice G_i , fallout of raindrops from the air parcel F_r , and fallout of ice particles F_i . The rising parcel is assumed to be saturated with respect to liquid water at all temperatures (i.e., entrainment and evaporation are ignored). Integration starts at cloud base ($z = 1$ km) where $q_c = q_v = q_r = 0$ and $q_v = q_s$. The lapse rate of the parcel was assumed to be 6 K km⁻¹ and temperature at 1000 hPa 291 K, based on the IOP2b soundings (Fig. 2). The fall speed of rain was set to 6 m s⁻¹ and the fall speed for ice was set to a value for graupel of 3 m s⁻¹. For a parcel above the 0°C level, the glaciation was assumed to be rapid,

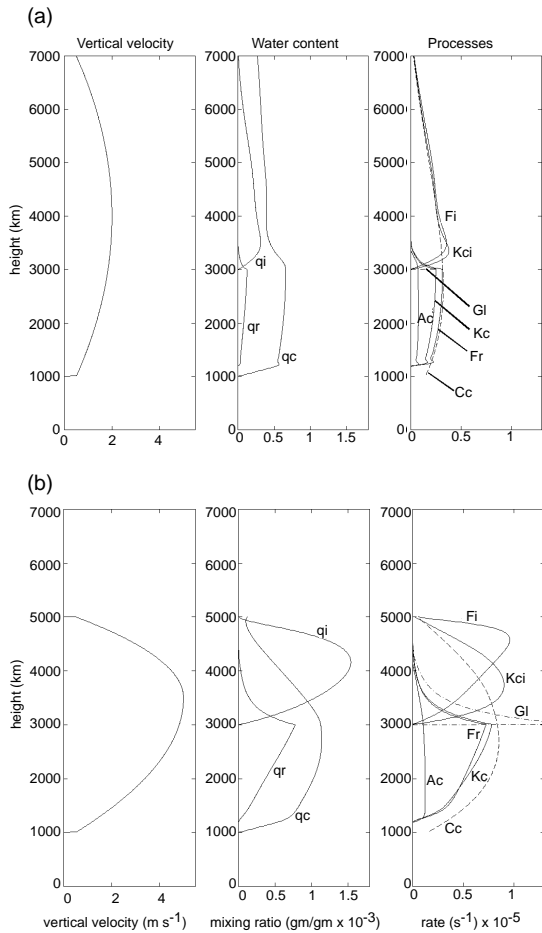


Figure 4. (a) Vertical velocity profile with max $w = 2 \text{ km s}^{-1}$ and updraft top of 7 km used as input to Kessler 1-D model (left panel). Vertical profiles of model output in terms of mixing ratios (middle panel) and precipitation process rates (right panel). See text for explanation of symbols and further details. (b) Similar to (a), except vertical velocity profile in the left panel with max $w = 5 \text{ km s}^{-1}$ and updraft top of 5 km used as input. (From Yuter and Houze 2001.)

such that by $\sim 1 \text{ km}$ above the 0°C level all the pre-existing rain had glaciated. Rapid glaciation is consistent with data obtained in several field studies (e.g., Yuter and Houze 1995; Zeng et al. 2001). The calculation is particularly sensitive to the assumptions regarding the glaciation rate and the fall speed relation of ice particles.

Several runs of the 1-D calculations were made using a parabolic profile of vertical air velocity from 1 to 7 km altitude and from 1 to 5 km altitude and assuming a 0°C level at 3-km altitude. Figure 4 shows the calculations for maximum w of 2 m s^{-1} for a velocity profile extending to 7-km altitude and for maximum w of 5 m s^{-1} within a velocity profile extending to 5-km altitude. The simplicity of the calculation limits our ability to make quantitative interpretations but some qualitative interpretations can be made. At weak-to-moderate vertical

velocities observed in MAP IOP2b precipitation, the 2-km thick layer above the freezing level contains local maxima in q_i and K_{Ci} , indicating that this region is a favorable growth environment for graupel. This result is consistent with the particle types inferred from the NCAR S-Pol radar in IOP2b (Fig. 3c). A comparison of the relative rates of K_C below the freezing level and K_{Ci} above the freezing level indicates that both collection of cloud water by rain and ice are important to the growth of precipitation and that neither can be ignored.

5. CONCEPTUAL MODEL

Figure 5 integrates the results from MAP IOP2a and IOP8, summarized in Secs. 2-4 above, into conceptual models of the orographic precipitation mechanisms in blocked and unblocked flows. In the blocked flow (Fig. 5a, based on IOP8), the low-level flow does not rise over the terrain. The flow above about the 1-km level

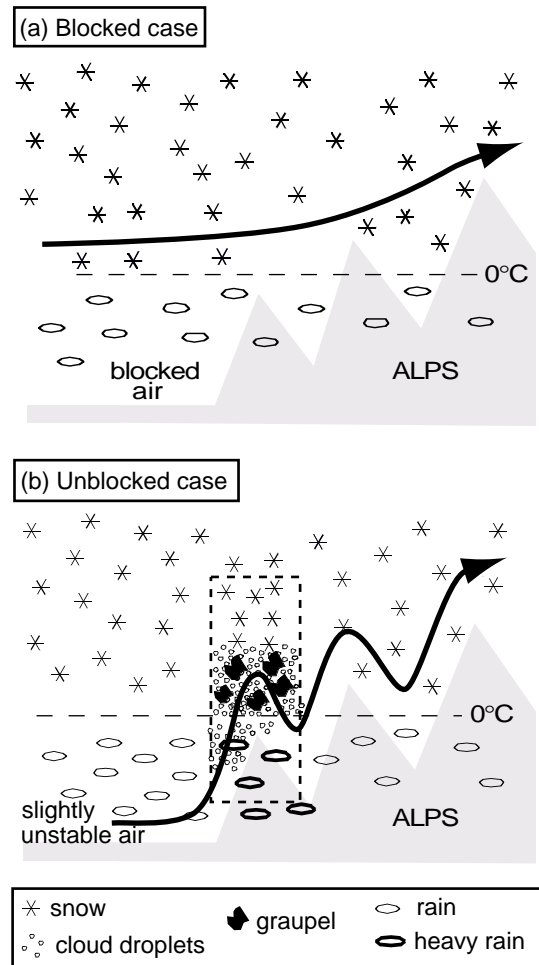


Figure 5. Conceptual model of the orographic precipitation mechanisms active in (a) blocked (b) unblocked flows. The diagrams show the types of hydrometeors present in each case, along with the behavior of the flow. Dashed box in (b) indicates position of embedded convective rainshower.

(~900 mb) rises over the windward slope but since the air was so stable, no convective cells formed. The resulting precipitation was entirely stratiform. Ice particles formed in the ascending flow, drifted downward, grew by vapor diffusion, and aggregated to form snowflakes, which melted and fell out as stratiform rain. The dominant particle growth mechanism in this scenario is vapor diffusion on ice particles (aggregation does not increase the mass of precipitation). The lifting is too gentle to produce enough liquid water for riming.

The unblocked case (Fig. 5b) contrasts sharply with the blocked case. There is a general background of stratiform cloud and precipitation, similar to that in the blocked case. However, since the static stability of the upstream flow is low, the entire layer of air, including the surface layer, rises easily up the terrain. The inclusion of the lower-level air, with its high vapor mixing ratio, in the air ascending over the windward slope of the range, makes the liquid water contents over the first peak of the terrain higher than in the blocked case. In addition, when the potentially unstable upstream air becomes saturated, convective cells are triggered in the upslope airstream. These cells, embedded in the background stratiform cloud and precipitation, produce especially high concentrations of cloud liquid water. As a result, raindrops grow rapidly by coalescence at low levels. Above the 0°C level, the cloud liquid water is supercooled, and ice particles in the upper parts of the cells grow by riming. The coalescence-grown raindrops and rimed ice particles fall out quickly over the peak of the terrain over which cells tend to be triggered. This cellularity embedded in the background stratiform precipitation leads to an efficient fallout of precipitation on the windward slopes.

6. CONCLUSION

Riming and coalescence of precipitation particles at low levels (as suggested by Fig. 5) appears to be a very important process in orographic precipitation. Hobbs et al. (1973) and Hobbs (1975) presented theoretical and observational evidence of the importance of riming in the lowest 1 km over the terrain frontal and postfrontal precipitation over the Cascade Mountains. The convective cells were small, but as in the case of MAP (Figs. 3a, c, and e, 4, and 5b), the cells provided enough supercooled water for graupel and other rimed particles to grow and fall out quickly on the windward side of the mountain barrier.

Caracena et al. (1979) showed from operational radar and sounding data that the Big Thompson flood on the eastern slope of the Rocky Mountains in 1976 occurred in a very unstable orographic upslope flow. When the strongly potentially unstable air was lifted, an intense thunderstorm ensued in a position tied to the windward-side topography. One of the signature features of the storm was the low-altitude reflectivity maximum (similar to the less-intense Alpine case in Fig. 3a). The authors hypothesized that growth of raindrops by coalescence was a primary reason for this storm structure.

MAP has provided modern radar data sets for the stable and weakly unstable cases of heavy orographic rain. Key data sets include the S-Pol polarimetric radar data, which allow detection of the preferred location of the formation of graupel particles, which indicate where riming tends to occur. Also important to the MAP analysis have been (1) the Doppler on Wheels, to observe the flow up and down valleys shielded from scanning radars; (2) airborne Doppler radar, to provide the broader mesoscale flow pattern; and (3) vertically pointing Doppler radar, to determine the updraft locations and intensities in convective cells over the mountains. Future studies should aim to obtain similar modern data sets in the strongly unstable cases. The mountains of Taiwan might provide a good venue for a field program with such an aim.

Acknowledgments: This research was supported by National Science Foundation grant number ATM 9817700.

REFERENCES

- Bougeault, P., P. Binder, A. Buzzi, R. Dirks, R. A. Houze, Jr., J. Kuettnner, R. B. Smith, R. Steinacker, and H. Volkert, 2001: The MAP special observing period. *Bull. Amer. Meteor. Soc.*, **82**, 433-462.
- Bousquet, O., and B. F. Smull, 2001: Comparative study of two orographic precipitation events exhibiting significant upstream blocking during MAP. *MAP Newsletter*, No. 15, 76-79. (Available from MeteoSwiss, Krähbühlstrasse 58, CH-8044, Zürich, Switzerland.)
- Caracena, F., R. A. Maddox, L. R. Hoxit, and C. F. Chappell, 1979: Mesoanalysis of the Big Thompson storm. *Mon. Wea. Rev.*, **107**, 1-17.
- Hobbs, P. V., 1975: The nature of winter clouds and precipitation in the Cascade Mountains and their modification by artificial seeding. Part I: Natural conditions. *J. Appl. Meteor.*, **14**, 783-804.
- Hobbs, P. V., R. C. Easter, and A. B. Fraser, 1973: A theoretical study of the flow of air and fallout of solid precipitation over mountainous terrain. Part II: Microphysics. *J. Atmos. Sci.*, **30**, 813-823.
- Houze, R. A., Jr., and S. Medina, 2001: Alpine precipitation mechanisms in MAP IOP2b and IOP8. *MAP Newsletter*, No. 15, 47-50. (Available from MeteoSwiss, Krähbühlstrasse 58, CH-8044, Zürich, Switzerland.)

- Houze, R. A., Jr., S. Medina, and M. Steiner, 2000: Two cases of heavy rain on the Mediterranean side of the Alps in MAP. Preprints, *Ninth Conf. on Mtn. Meteor.*, Aspen, CO, Amer. Meteor. Soc., 1-5.
- Smith, R. B., 1979: The influence of mountains on the atmosphere. *Advances in Geophysics*, **21**, 87-230.
- Smull, B., O. Bousquet, and D. Lüthi, 2001: Evaluation of real-time MC2 simulation results for a case of significant upstream blocking during MAP. *MAP Newsletter*, No. 15, 84-87. (Available from MeteoSwiss, Krähbühlstrasse 58, CH-8044, Zürich, Switzerland.)
- Vivekanandan, J., and Coauthors, 1999: Cloud microphysics retrieval using S-band polarization radar measurements. *Bull. Amer. Meteor. Soc.*, **80**, 381-388.
- Yuter S. E., and R. A. Houze, Jr., 1995: Three-dimensional kinematic and microphysical evolution of Florida cumulonimbus. Part II: Frequency distributions of vertical velocity, reflectivity, and differential reflectivity. *Mon. Wea. Rev.*, **123**, 1941-1963.
- Yuter, S. E., and R. A. Houze, Jr., 2001: Microphysical modes of precipitation growth determined by vertically pointing radar at Locarno-Monti during MAP. *MAP Newsletter*, No. 15, 110-113. (Available from MeteoSwiss, Krähbühlstrasse 58, CH-8044, Zürich, Switzerland.)
- Zeng, Z., S. E. Yuter, R. A. Houze, Jr., and D. E. Kingsmill, 2001: Microphysics of the rapid development of heavy convective precipitation. *Mon. Wea. Rev.*, **129**, 1882-1904.